REPORT DOCUMENTATION PAGE

Form Approved
OMB No. 0704-0188

Public reporting burden for this collection of information is estimated to average 1 hour per response, including the time for reviewing instructions, searching existing data sources, gathering and maintaining the data needed, and completing and reviewing this collection of information. Send comments regarding this burden estimate or any other aspect of this collection of information, including suggestions for reducing this burden to Department of Defense, Washington Headquarters Services, Directorate for Information Operations and Reports (0704-0188), 1215 Jefferson Davis Highway, Suite 1204, Arlington, VA 22202-4302. Respondents should be aware that notwithstanding any other provision of law, no person shall be subject to any penalty for failing to comply with a collection of information if it does not display a currently valid OMB control number. **PLEASE DO NOT RETURN YOUR FORM TO THE ABOVE ADDRESS.**

1. REPORT DATE (DD-MM-YYYY) June 2014	2. REPORT TYPE Technical Paper	3. DATES COVERED (From - To) June 2014- July 2014
4. TITLE AND SUBTITLE Interpretation of Core Length in Shear Coaxial Rocket Injectors from X-ray Radiography Measurements		5a. CONTRACT NUMBER In-House
		5b. GRANT NUMBER
		5c. PROGRAM ELEMENT NUMBER
6. AUTHOR(S) S.A. Schumaker, A.L. Kastengren, M.D.A. Lightfoot and S.A. Danczyk		5d. PROJECT NUMBER
		5e. TASK NUMBER
		5f. WORK UNIT NUMBER Q0X3
7. PERFORMING ORGANIZATION NAME(S) AND ADDRESS(ES) Air Force Research Laboratory (AFMC) AFRL/RQRC 10 E. Saturn Blvd. Edwards AFB CA 93524-7680		8. PERFORMING ORGANIZATION REPORT NO.
9. SPONSORING / MONITORING AGENCY NAME(S) AND ADDRESS(ES) Air Force Research Laboratory (AFMC) AFRL/RQR 5 Pollux Drive Edwards AFB CA 93524-7048		10. SPONSOR/MONITOR'S ACRONYM(S)
		11. SPONSOR/MONITOR'S REPORT NUMBER(S) **AFRL-RQ-ED-TP-2014-173**

12. DISTRIBUTION / AVAILABILITY STATEMENT Distribution A: Approved for Public Release; Distribution Unlimited

14. ABSTRACT
Shear coaxial injectors are so named because they rely on the shear between an outer lower-density high velocity annulus and a higher-density low-velocity inner jet to atomize and mix a liquid and a gas. These injectors have an intact core, and the high amount of scatter its corrugated surface produces creates large optical densities. These high optical densities, in turn, make interrogation of the spray field in the region of the core difficult. In combustion applications, such as rockets, this region is also the area of flame holding, so is of primary importance in predicting combustion behavior. To overcome the problems of multiple scattering, the near-injector region was studied using X-ray radiography at Argonne National Laboratory's Advanced Photon Source. These results clearly show regions of differing behavior throughout the downstream distance examined. These regions correspond to changes in atomization behavior and can be used to quantify "core length" and understand more clearly what this term means. Three methods are explored to measure core length from X-ray radiography data and are compared to two-phase core length measurements from the literature. The core length non-dimensionalized by the inner jet diameter was found to scale with the momentum flux to the -0.66 power.

15. SUBJECT TERMS

16. SECURITY CLASSIFICATION OF:			17. LIMITATION OF ABSTRACT	18. NUMBER OF PAGES	19a. NAME OF RESPONSIBLE PERSON A.Schumaker
a. REPORT **Unclassified**	b. ABSTRACT **Unclassified**	c. THIS PAGE **Unclassified**	SAR	17	19b. TELEPHONE NO (include area code) 661-275-5165

Standard Form
298 (Rev. 8-98)
Prescribed by ANSI
Std. 239.18

Interpretation of Core Length in Shear Coaxial Rocket Injectors from X-ray Radiography Measurements

S. Alexander Schumaker[1], Stephen A. Danczyk[2] and Malissa D.A. Lightfoot[2]
Air Force Research Laboratory, Edwards AFB, CA, 93524

Alan L Kastengren[3]
Argonne National Laboratory, Argonne, Illinois 60439

Shear coaxial injectors are so named because they rely on the shear between an outer lower-density high-velocity annulus and a higher-density low-velocity inner jet to atomize and mix a liquid and a gas. These injectors have an intact core, and the high amount of scatter its corrugated surface produces creates large optical densities. These high optical densities, in turn, make interrogation of the spray field in the region of the core difficult. In combustion applications, such as rockets, this region is also the area of flame holding, so is of primary importance in predicting combustion behavior. To overcome the problems of multiple scattering, the near-injector region was studied using X-ray radiography at Argonne National Laboratory's Advanced Photon Source. These results clearly show regions of differing behavior throughout the downstream distance examined. These regions correspond to changes in atomization behavior and can be used to quantify "core length" and understand more clearly what this term means. Three methods are explored to measure core length from X-ray radiography data and are compared to two-phase core length measurements from the literature. The core length nondimensionalized by the inner jet diameter was found to scale with the momentum flux to the -0.66 power.

Nomenclature

A	=	Jet area
D	=	Jet diameter
I	=	Intensity of transmitted radiation
I_o	=	Intensity of incident radiation
J	=	Momentum flux ratio, $\rho_g U_g^2 / \rho_l U_l^2$
L	=	Jet inlet length
L_c	=	Inner jet core length
L_p	=	Pathlength of beam
m	=	Mass flux ratio, $\rho_l U_l A_l / \rho_g U_g A_g$
$\dot{m}$	=	Mass flow rate
Oh	=	Ohnesorge number, $\mu_l/(\rho_l \sigma_l D_l)^{1/2}$
Re_g	=	Gas Reynolds number, $U_g(D_g-(D_l+2T_p))/\nu_g$
Re_l	=	Liquid Reynolds number, $U_l D_l / \nu_l$
r	=	Radial coordinate
x	=	Downstream coordinate
T	=	Thickness
U	=	Velocity
We	=	Weber number, $\rho_g U_g^2 D_l/\sigma$
Φ	=	Mass flux
β	=	Mass attenuation coefficient
ρ	=	Density
σ	=	Surface tension
ν	=	Kinematic viscosity
μ	=	Viscosity

---

[1] Research Engineer, RQRC, Senior Member AIAA.
[2] Research Scientist, RQRC, Member AIAA.
[3] Research Engineer, Energy Systems Division, Member AIAA.

American Institute of Aeronautics and Astronautics

Subscripts

g	=	Gas
l	=	Liquid
ma	=	Mass averaged
p	=	Injector post
rms	=	Root-mean-square

I.   Introduction

Due to their utility in a number of combustion devices (turbofan engine exhaust, air blast furnaces, and liquid rocket engines) shear coaxial jets have been studied for over sixty years and have become a canonical problem for the study of rocket injector dynamics.[1] Shear coaxial injectors rely on the shear between an outer lower-density high-velocity annulus and a higher-density low-velocity inner jet to atomize and mix a liquid and a gas. In all applications the complex near field (two annular shear layers in close proximity) is of critical importance in determining system performance. In rocket engines, shear coaxial jets have been used as injectors for both boost class engines (SSME, Ariane 5)[2, 3] and upper stage engines (J-2).[4] Shear coaxial jets work well with propellant combinations and engine cycles that produce significant shear at reasonable pressure drops, such as H_2/LOX or CH_4/LOX engines using a fuel regeneratively-cooled combustion chamber.

Previous coaxial jet research can be divided by the phase of the two fluids as either single or multiple phases. Much of the fundamental coaxial jet research has been done using a single phase (either gas-gas or liquid-liquid mixing). A brief review of single-phase coaxial jet research can be found in Schumaker and Driscoll[5]. Single-phase cases also include work where both fluids are supercritical, which is common in modern boost-class liquid rocket engines. Studies have indicated that "liquid-core" coaxial jets operating at supercritical conditions scale in a similar manner to single-phase coaxial jets. However, details and scaling constants differ.[6]

The second class of coaxial jets operate with two different fluid phases. The gaseous high-speed outer jet (fuel) is used to fragment a dense liquid core (oxidizer). This fluid configuration is common in upper-stage rocket engines and during throttled conditions, start-up and shut-down transients of boost-class engines. The current work focuses on this multiphase type of jet. An excellent review on coaxial jet atomization can be found in an article by Lasheras and Hopfinger.[7] In these previous studies, optical imaging techniques have been used to study the liquid core breakup process and measure global spray structures such as liquid core length and spray angle.[8, 9] On the spray periphery and in the fair-field PDPA has been used to measure droplet sizes and velocities.[9] From these measurements regime diagrams have been developed along with scaling laws for the liquid core length and empirical correlations for spray angles and droplet distributions in the far field.[7, 9, 10] The current study looks to understand how core lengths of shear coaxial jets measured from X-ray radiography data compare with core lengths measured from optical imaging data reported in the literature. Comparing data from a newly applied technique, X-ray radiography, to the well-studied problem of core length of shear coaxial jets is an important step in understanding the strengths and weakness of the new measurement technique.

In the past the exploration of the near-field region of dense sprays, such as the current coaxial jets, has been hampered by the elastic scattering that dominates visible-light measurement techniques or by perturbation of the flow field through intrusive measurements. X-ray radiography overcomes both of these issues, since the dominate interaction of photons in the X-ray part of the spectrum with droplets is absorption. Beer's law can be used to solve for a path integrated liquid-phase thickness or projected density, which provides a quantitative measure of the mass density at any location in the spray. Integrating a cross-sectional profile of the spray and dividing by the liquid-mass-flow rate allows a mass averaged velocity to be calculated.

In the recent years X-ray radiography has shown its usefulness by successfully interrogating the near field of a number of dense sprays including diesel injectors, aerated liquid jets, solid-cone sprays, impinging-jet sprays and gas-centered swirl-coaxial injectors.[11-15] While X-ray radiography can be performed using a synchrotron source or a tube source, a synchrotron source has a number of well-documented advantages over a tube source, notably possessing sufficient flux to produce a monochromatic beam.[16] The one large disadvantage of a synchrotron source is that the experiment must be brought to a synchrotron facility, and these facilities lack spray infrastructure. The issues of spray infrastructure have been largely overcome by the development of a mobile test rig that can deliver high flow rates and pressures of gaseous nitrogen and water while integrated into the 7-BM beamline of the Advanced Photon Source (APS) located at Argonne National Laboratory.

The present study uses time-averaged and time-resolved X-ray radiography to measure centerline and radial profiles of Equivalent Path Length (EPL) or the projected liquid phase density in shear coaxial jet injectors. Three

methods are explored to measure an inner jet core length from the centerline profiles, percentage decrease in the EPL normalized by the inner jet diameter, the change in spatial derivative of EPL, and the maximum RMS. Core lengths obtained using these methods are then compared to core length data from the literature, and scaling laws for the current data set are derived.

II.   Experimental Methods

X-ray radiography measurements were performed at the 7-BM beamline at the Advanced Photon Source. The X-ray source for the beamline is a synchrotron bending magnet. This source produces polychromatic, nearly collimated radiation. A double-multilayer monochromator is used to produce a monochromatic ($\Delta E/E=1.4\%$) X-ray beam. Details regarding the beamline setup are given in Ref. 17. For the current experiment a beam photon energy of 10 keV was used. Using a pair of Kirkpatrick-Baez focusing mirrors housed in the experimental enclosure the beam was focused to 7 µm vertical x 8 µm horizontal (full width at half maximum) at a flux of 1.6×10^{10} photons per second before the experimental apparatus. A silicon PIN diode was used as the detector. A sketch of the experimental setup is shown in Fig. 1. The photocurrent from this PIN diode was amplified and time averaged over to produce time-averaged data. Time-resolved data was collected from the same diode at (at a different time than the time-averaged data) 6 MHz and was used to generate root mean square profiles of the EPL. One-dimensional transverse scans were made across the spray, perpendicular to the injector axis with a 0.25 mm step size. One-dimensional scans were also made on the spray centerline, parallel to the injector axis with a 0.25 mm step size. Radial scan widths varied between 8 and 16 mm depending on test condition and downstream location, selected to minimize data collected outside the spray. Centerline scan were conducted between 0.25 and 25 mm downstream. For every flow condition, radial scans were performed 0.02, 0.5, 1, 2.5, 5, 10, 15 and 25 mm downstream of the injector face. Injector rotations were performed for only a single experimental condition due to the high level of symmetry in the radial profiles observed for all test conditions.

The recorded signal level was converted to the Equivalent Path Length (EPL) of water using Beer's law,

$$EPL = \frac{-\ln(I/I_0)}{\beta \rho_l},\qquad(1)$$

where I is the intensity of the transmitted light, I_0 is the intensity of incident light, β is the mass attenuation coefficient, and ρ_l is the density of the absorbing fluid (in this case demineralized water). Normalization by I_0 was performed in two steps. First, each point in the scan was normalized by a corresponding beam intensity measured from an intensity monitor based on fluorescence from a thin titanium foil placed inline with the beam upstream of the spray. The I_0 measurement accounts for changes in beam intensity during a scan. The second normalization baselines the intensity to the zero absorption case (no water in the beam) and uses the average signal level from the 5 points in the scan with the highest transmissions, points outside of the spray. Since centerline profiles (i.e. those parallel to the spray axis) contained no points outside of the spray, the centerline profiles were normalized using the same baselines as the 10 mm downstream radial (i.e. cross-axis) profile.

The mass attenuation coefficient can be calculated using the NIST photon cross-section database;[18] for pure water and a beam energy of 10 keV, $\beta=5.33$ cm^2/g. Gas phase absorption is much less than the liquid phase absorption, therefore, the reduction in absorption is almost entirely due to the liquid phase mass. The EPL is the pathlength-integral of the amount of water in the beam. EPL can be roughly conceptualized as the thickness of water that is in the beam, on average, over a given time period. Again, for the time-averaged data this time period is several seconds while the time period is a 0.16 microseconds for the time-resolved measurements. In terms of flow variables, time averaged EPL is a function of the local mass flux and velocity. For an area of uniform mass flux and liquid phase velocity

$$EPL = \frac{\Phi L_p}{U_l \rho_l},\qquad(2)$$

where Φ is the mass flux, U_l is the velocity of the liquid phase, and L_p is the pathlength of the area. If the only data available is time-averaged EPL, then changes in velocity cannot be distinguished from changes in mass flux. Additional information to differentiate the two could come from other techniques, such as mechanical patternation; however, mechanical patternation is difficult to perform in the near field of dense sprays without altering the flowfield. It should be noted that the use of monochromatic X-rays greatly simplifies the conversion of X-ray transmission to EPL; this is a significant advantage of synchrotron sources over laboratory X-ray sources.

Surrogate propellants (water and gaseous nitrogen) were delivered to the injector using a facility dubbed the Mobile Flow Laboratory (MFL). The MFL was designed to allow aerospace-propulsion injector testing at remote diagnostic facilities such as the APS that do not have the infrastructure to provide relevant flow conditions. The MFL is a self-contained system with its own data acquisition and control systems, allowing it to be run remotely. Liquid nitrogen, electrical power and an exhaust system are all that is required of the host facility. Gaseous nitrogen is produced from the liquid supply and is stored in two, 57-liter gas bottles. The gaseous nitrogen is also used to pressurize a 57-liter water tank. Gas and liquid flow rates are controlled using electronic pressure regulators with calibrated critical flow orifices. The system has an uncertainty of 4% in the gas flow rate and 1% in the liquid flow rate.[19]

Four shear-coaxial jet injector geometries were used in the current study. These injectors are scaled-up versions of injectors previously used by AFRL to study supercritical and acoustic effects on shear coaxial jets.[20, 21] The injectors used in the current study were enlarged using photo scaling to increase X-ray absorption and to better fit the mass flow capabilities of the Mobile Flow Laboratory. A schematic of the injector geometries are shown as Fig. 2, and a photo of the injector assembly is provided as Fig. 3. Table 1 lists critical injector dimensions. In all cases liquid H_2O flows from the inner jet and gaseous N_2 from the outer jet. This propellant arraignment is representative of LOX flowing for the inner jet and vaporized CH_4 or H_2 from the outer jet. Due to space constraints in the test hutch, injectors were run in a horizontal orientation.

III. Scaling & Test Matrix

Previous studies have shown that two-phase coaxial jets' stability and atomization are controlled by six nondimensional parameters.[7] These parameters are the liquid and gas Reynolds number (Re), the Ohnesorge number (Oh), the Weber number (We), the momentum flux ratio (J), and the mass flux ratio (m). Full definitions are provided in the nomenclature. In the current study the main parameters of interest are J and m. The mass flux ratio is defined as liquid to gas while the momentum flux ratio is defined as gas to liquid. The current test conditions were compared against the shear coaxial atomization regime diagram developed by Lasheras and Hopfinger[7], which is reproduced in Fig. 4 with the locations of the current test conditions overlaid. From Fig. 4 it is clear that all conditions are within the fiber-type breakup regime. Since all flow conditions investigated here are in the same atomization regime and the other nondimensional parameters (Re_g, Re_l, Oh, and We) vary minimally, only changes in J and m are expected to have an observable impact. In the jet near-field the shear, or nondimensionally the momentum flux ratio, between the two fluids controls primary atomization. The mass flux ratio plays a role in the primary atomization region through the included inner jet to outer jet area ratio for small values of the area ratio. The area ratio, along with the post thickness, sets the distance between the outer and inner shear layers. The distance between the two shear layers plays a role in if and how the layers couple and complete for mass entrainment. The mass flux ratio also affects secondary atomization and spray velocities by setting the relative amount of momentum that can be transferred from the gas to the liquid phase. The same jet velocities were used for the matching momentum flux ratio test condition; therefore, a difference in the mass flux ratio is due solely to changes in the area ratio.

One geometric variable that is not accounted for in these six nondimensional parameters is the post thickness T_p. The post thickness' primary effect is to set the size of the post-tip recirculation zone which, indirectly, sets the boundary conditions for the interaction between the two fluid streams and can play a significant role in setting the core length. For cases with thick post lips Teshome et. al showed that the core length scales with J, the outer to inner jet area ratio, and the post thickness nondimensionalized by the inner jet diameter.[23]

Flow conditions for each test case are provided in Table 2. For each injector geometry five nominal momentum flux ratio conditions were run (J=0.5, 2, 5, 10, 15). Flow velocities were set so that the gas-jet Mach number was always less than 0.7.

IV. Results and Discussion

Throughout the literature the terms core, potential core and dark core are used to describe the inner jet core of two-phase shear coaxial jets. Dark core is typically used to describe a core length measured using backlit imaging techniques while potential core is typically used to refer to a core length measured from velocity data. For the current work core length will be used to describe a length measured from any data type. Note that if two different measurement techniques are both measuring the same core length type then the observed trends for both techniques should be the same and any difference in scaling laws should be limited to a change in a scalar constant. Exponents

which mathematically describe the trend should be the same. Any difference in the exponent or scaling relation other than the scalar constant indicates that the two techniques are measuring different structures in the spray.

Figure 5 shows normalized centerline and radial EPL profiles for injectors SC24 and SC1. These profiles are representative of the data taken at all test conditions. Figure 5a shows the centerline profiles for injector SC24 at five momentum flux ratio (J) conditions. As expected from the scaling laws in the literature, as J is increased the breakup of the inner jet is increased so that the EPL decreases in a shorter downstream distance. From the centerline profiles it is also clear that none of the test conditions start exactly at $EPL/D_i=1$. A value of one is representative of the inner jet leaving the injector-body as a perfect cylinder. Values above one indicate liquid trapped in the injector-tip recirculation zone. The amount of recirculating liquid can become quite significant, as in the case of injector SC1 which has a very thick injector post tip. Figure 6b is an instantaneous backlit image of test condition SC1-10 which shows a significant amount of recirculating liquid at the injector post tip. In comparison Fig. 6a shows minimal recirculating liquid in the much thinner injector post of injector SC4. Initial values of EPL below one indicate either a necking down of the inner jet at the injector exit or rapid atomization.

Figures 5b and 5c are normalized radial EPL profiles for injectors SC24 and SC1. Close to the jet exit the EPL profiles of SC24-10 have an elliptical shape due to the shape of the liquid jet core, elliptical EPL is what would be expected from a cylinder of liquid and has previously been observed in diesel injector studies.[12] SC1-10, Fig. 5b, departs from this elliptical shape due to the large recirculation zones at the injector post. The partially atomized mass in the injector tip recirculation adds shoulders to the radial EPL profiles. Farther downstream both the sprays widen and the total EPL drops as the core is atomized and the droplets are accelerated by the higher-velocity outer-gas stream. As noted in the Experimental Methods section, the EPL is a function of both the mass flux and velocity for droplet-laden flows. Equation 2 indicates that EPL can decrease due to decreasing mass flux or increasing droplet velocity. While the decrease in EPL at the downstream locations is partially due to spray spreading, the more significant factor causing the significant decrease in EPL is the acceleration of the droplets to higher velocities. In the current work liquid exit velocities are between 2-6 m/s while gas exit velocities vary between 81-229 m/s.

Visible in the centerline EPL profiles are distinct regions characterized by significant differences in slope. It is hypothesized that these distinct regions can be used to distinguish different atomization or spray breakup regions in the flow. Figure 7 shows two centerline EPL profiles for injector SC4 with four hypothetical regions labelled. The first region is the near-injector region which is characterized by either a constant or slight increase in the centerline EPL immediately following the injector exit. In the case of the thick lip configuration, SC1, this region can extend up to three times the jet diameter, as is shown in Fig. 8a. The near-injector region exists due to boundary conditions created by the post geometry that delays interaction of the two streams. The shape of this near-injector region and/or its existence is governed by J, the injector post geometry, and the jet exit velocity profiles. The two largest drivers are the post recirculation zone and the velocity boundary layers at the jet exit.

The second region, and the primary focus of this work, is the primary atomization region, or the core breakup region, which is characterized by the initial area of nearly linear decline in EPL. The slope of this section is related to the atomization rate and, therefore, is largely controlled by J. The post thickness or more specifically the size of the recirculation zones can also play a role, as is evident in Fig. 8a for the SC1. Unfortunately the X-ray radiography technique cannot distinguish between intact liquid in the jet and droplets. The core breakup region is the most investigated region in shear coaxial jets, due to the importance it plays in setting and controlling the primary combustion zone. Another reason is that backlit imaging techniques can be used to measure the core length.

The third region shown by the centerline EPL profiles is the transition between core breakup and the far-field. The transition region is characterized by a clear change of slope in the centerline profiles. As J increases the length of the transition region decreases and the change in slope becomes more abrupt. The last region observed here is the far-field zone where drop acceleration is occurring along with some secondary atomization. EPL continues to decrease and the spray widens, droplets break apart and accelerate to higher velocities. This region again has nearly linear slope. This region has received relatively less study for propulsion applications since combustion will severely alter droplet sizes in this region.

This atomization regime concept raises the logical question of how these regions scale? As the first step to answering this question, the scaling of the core breakup region was investigated. Existing literature data on the core length of two-phase shear coaxial jets can be leveraged in this region. Three methods were explored to measure the inner jet core length from the centerline X-ray radiography data, percent decrease in EPL, change in slope by calculating the first spatial derivative of EPL, and the peak EPL RMS.

The percent decrease in centerline EPL is attractive because, after normalization, it can be uniformly applied to all conditions and geometries. This method resembles using a stoichiometric mixture ratio to define a mixing length, but no theory exists to recommend a meaningful percent decrease to choose in the atomization case. The centerline EPL profiles collected, provided as Fig. 8 for all test conditions, do suggest a range of likely values. Values of

EPL/D$_i$ above 0.7 were found to depend highly on the near injector region. Values of *EPL/D$_i$* below 0.2 were largely found to have transitioned to the far-field breakup region. This range of values was explored by plotting core length (*L$_c$*) versus *J* across the range at 0.1 increments. Results are provided visually as Fig. 9. As would be expected, Fig. 9 shows an increase in core length with decreasing *EPL/D$_i$* ratio for all J values.

The change in slope, first spatial derivative, of the EPL should capture the departure from the nearly linear trend of the core breakup region to the nonlinear behaviour in the transition region (Fig. 7). The human eye is adept at noticing these changes, but spatial derivatives can be sensitive and noisy when applied to experimental data making the determination of a transition point difficult. To ease these challenges, the experimental data was smoothed prior to calculating the derivative. A running average over 5 points was chosen because it provided sufficient smoothing and produces less uncertainty than the other smoothing techniques. The resulting derivative, calculated using a 4 point centered finite-divided-difference formula, is shown in Fig. 10 for all conditions and geometries. The results in Fig. 9 illustrate the discrepancy between human perception and mathematical processing. Observation creates an expectation of a nearly constant derivative over the core breakup region followed by a sharp decrease in the transition region. However, none of the test cases show this trend because the "nearly" linear behaviour in the core region is an approximation to which derivative calculations are very sensitive. Except in cases where little or none of the far field was captured, Fig. 10 shows that it would be possible to determine the beginning of the far field behaviour by setting a lower threshold derivative. The results would give an estimate of the core and transition regions together. These values would be expected to exceed the core lengths calculated with the other methods but meaningful comparisons beyond that would not be straightforward. As a result, the calculated core plus transition lengths from the derivative technique are not discussed further.

The time-resolved results enable the calculation of a Root-Mean-Square (RMS) of the EPL signal. The time-resolved data were taken at 6MHz at a separate instance in time from the time-averaged data. The average of the time-resolved data was found to agree well with the hardware averaged data. As previously mentioned, EPL has a dependence on both the mass flux and the velocity of the liquid phase (Eqn. 2) and, therefore, dynamic slow moving liquid structures with the high mass flux will be the largest contributors to the RMS signal. As shown in Fig. 4, all conditions examined here were in the fiber-type breakup regime described by Lasheras and Hopfinger.[7] In this regime aerodynamic forces dominate over surface tension forces and surface disturbances are easily amplified and eventually broken up into droplets. The surface of the liquid core has many disturbances that are of varying sizes due, in part, to being at different stages in the amplification and breakup process. In areas where the liquid core is partially atomized, droplets are still being created and undergoing secondary atomization. Due to the high aerodynamic forces on the droplets in this regime they quickly accelerate decreasing there impact on the RMS. High RMS values are, therefore, caused by surface features such as waves and ligaments along with core tip unsteadiness which cause the tip to move in and out of the beam path. On the centerline, it is hypothesized that the peak RMS corresponds with the tip of the liquid core.

Centerline RMS profiles for all conditions are provided in Fig. 11. Clear peaks in the profiles are observable in all higher momentum flux ratio cases. For all *J=0.5* cases and the *J=1.8* and *J=4.5* conditions for SC2, data were not taken sufficiently far downstream to capture the peak. Using the downstream location of the peak value as the core length, a comparison was made with the percent EPL core lengths. It was found the lengths measured using the peak RMS values showed excellent agreement with the *EPL/Di=0.3* lengths. The comparison of these two core length measurement is shown in Fig. 12 for the SC4 geometry. While the comparison is only shown for the SC4 similar agreement was observed for all injector geometries. Given this agreement in core length between the two methods it was decided to use the 30% EPL core length data to develop scaling laws and for comparison with literature values.

A comparison of the current coaxial jet core length data with that of three prior two-phase studies was made and is provided as Fig. 13. Figure 13 shows a clear difference in scaling between the current data and that of Leyva et. al.[26] The data from Woodward et. al.[24] and Eroglu et. al.[25] were taken at lower *J* values and overlaps with the current data set and that of Leyva et. al. over only a small range of *J* Values. Reasonable best fit lines can be calculated for the current or the Leyva et. al. data sets in combination with the Woodward et. al. and Eroglu et.

al. data sets. Due to the greater overlap of the Leyva et. al. data set with that of Woodward et. al. a high confidence should be placed on the Leyva et. al. data set. This observed difference leads to the logical question of what is the cause of this discrepancy? One possibility is the differences in measurement techniques. The current studied utilized X-ray radiography to measure core lengths while Leyva et. al. used backlit imaging. These two methods could be measuring different structures since the decrease in the X-ray signal is due only to mass absorption while the decrease in signal used to measure core length for backlit imaging is due primary to multiple scattering effects. It should be noted that Eroglu and Chigier made their measurements using backlit imaging while Woodward et. al. made their measurements using X-ray radiography. The X-ray imaging method used by

American Institute of Aeronautics and Astronautics

Woodward et. al. is different from the technique shown here. Woodward et. al utilized a polychromatic laboratory X-ray source. Calibration cells with different thicknesses of liquid (KI-solution) were imaged. The spray was then imaged and a liquid thickness was chosen to correspond to the end of the potential core. Using the signal from the calibration cells a thresholding technique was then applied and the core length was measured from the binary image.[24] It is unclear at this time how the thresholding method used by Woodward et. al. compares with the methods used in the current work. In the future backlit images of the current test conditions will be obtained allowing for direct comparison of the two methods.

Three methods were explored to scale the core length data. The first is the standard momentum flux ratio scaling which is simply a constant times the momentum flux ratio to a power.[7, 26] The best fit to this model using linear regression is shown in Fig. 14a. Using this method it was found that the current data scales with the momentum flux ratio to the -0.66 power. This value differs significantly from the momentum flux ratio to the -0.2 power suggested by Leyva et. al.[26] for two-phase coaxial jets. This finding more closely agrees with the commonly used momentum flux ratio to the -0.5 scaling for single-phase coaxial jet. Given the large variation in injector post thickness and area ratio between the injector geometries the scatter seen in Fig. 14a is not entirely unexpected. The amount of scatter can be reduced by including the post thickness to inner diameter ratio and the area ratio in the scaling as suggested by Teshome[23] (Fig. 14b). The correlation suggested by Teshome provides the best collapse of the three methods. The last method explored was that suggested by Lasheras and Hopfinger[7] and includes the momentum flux ratio to the -0.5 power and the liquid to gas velocity ratio. For the current conditions the velocity ratio was always less this 0.05 and therefore, had little to no effect reducing the scaling law to $9J^{-.5}$. The Lasheras and Hopfinger's scaling law applied to the current data is shown as Fig.14c. Interestingly the method suggested by Lasheras and Hopfinger works best for the largest (SC1) and smallest (SC2) area ratio injectors tested.

V. Summary and Conclusions

Single point X-ray radiography was used to obtain quantitative equivalent pathlength measurements (EPL) in shear coaxial rocket injectors. Both radial and centerline EPL profiles were obtained for 4 injector geometries and 5 momentum flux ratio conditions spanning from 0.5 to 15. All test conditions were shown to be in the fiber-type atomization regime. Centerline profiles were used to develop four hypothetical atomization regions. As a first step in answering the question of scaling these atomization regions, the core breakup region was investigated. Three methods were investigated to define a core length from the centerline EPL profiles. These methods were percent decrease in EPL, change in slope by calculating the first spatial derivative of EPL, and the peak EPL RMS. The change in slope was found to be sensitive to measurement noise and only a length that included the transition region could be accurately defined. Core lengths obtained using a 30% decrease in EPL and the peak EPL RMS criteria showed excellent agreement with each other. Using the 30% decrease criteria, core length data from all test conditions were scaled using three methods. Using a simple momentum flux ratio scaling core, length data was found to scale with $J^{-0.66}$ which differs from the $J^{-0.2}$ scaling suggested by another investigation for two-phase coaxial jets. The $J^{-0.66}$ more closely agrees with the $J^{-0.5}$ scaling commonly used for single phase coaxial jets. A better collapse was obtained when the post thickness and area ratios were included in the scaling law. Direct comparison of the current core length data was made with three studies from the literature which further highlighted the difference in scaling between the current and prior studies. Two reasons for the discrepancy in scaling were explored including differences in what is being measured with X-ray radiography and backlit imaging and unaccounted for differences in the flow conditions. In the future backlit images of the current test conditions will be obtained so that direct comparison of core lengths measured from X-ray radiography and backlit imaging can be made. This additional work is needed to further understand the strengths and weakness of the X-ray radiography technique and how it compares with prior investigations.

VI. Acknowledgements

References

[1]Forstall, W., and Shapiro, A.H., "Momentum and Mass Transfer in Coaxial Gas Jets," *Journal of Applied Mechanics*, Vol. 17, No. 4, 1950, pp. 399-408.

[2]Sutton, G.P., and Biblarz, O., *Rocket Propulsion Elements: An Introduction to the Engineering of Rockets*, 7th ed., Wiley Interscience, 2001.

[3]Juniper, M., Tripathi, A., Scouflaire, P., Rolon, J.-C., and Candel, S., *Sixth International Conference on Liquid Atomization and Spray Systems*, Edinburgh, Scotland, 2000, pp. 1103-1109.

[4] Young, V. & Anderson, W.E. (Ed.), *Liquid rocket engine combustion instability*, Vol. 169, AIAA, 1995.

[5]Schumaker, S.A., and Driscoll, J.F., "Mixing Properties of Coaxial Jets with Large Velocity and Large Inverse Density Ratios," *Physics of Fluids*, Vol. 24, No. 5, 2012, 055101.

[6]Davis, D.W., Chehroudi, B., and Talley, D.G., "A Rocket-Like Coaxial Injector in and Acoustic Field under Sub- and Supercritical Conditions," *10th International Congress on Liquid Atomization and Spray Systems*, Kyoto, Japan, 2006.

[7]Lasheras, J.C., and Hopfinger, E.J., "Liquid Jet Instability and Atomization in a Coaxial Gas Stream," *Annual Review of Fluid Mechanics*, Vol.32, 2000, pp. 275-308.

[8]Davis, D.W., and Chehroudi, B., "Measurements in an Acoustically Driven Coaxial Jet under Sub-, Near-, and Supercritical conditions," *Journal of Propulsion and Power,* Vol. 23, No. 2, 2007, pp. 364-374.

[9]Lasheras, J.C., Villermaux, E., and Hopfinger, E. J., "Break-up and Atomization od a Round Water Jet by a High-Speed Annular Air Jet," *Journal of Fluid Mechanics*, Vol. 357, 1998, pp. 351-379.

[10]Rehab, H., Villermaux, E., and Hopfinger, E. J., "Flow Regimes of Large-Velocity-Ratio Coaxial Jets," *Journal of Fluid Mechanics*, Vol. 345, 1997, pp. 357-381.

[11]Leick, P., Kastengren, A.L., Liu, Z., Wang, J., and Powell, C.F., "X-ray Measurements of Mass Distributions in the Near-Nozzle Region of Sprays form Standard Multi-hole Common-rail Diesel Injection Systems," *11th Triennial International Conference on Liquid Atomization and Spray Systems*, Vail, Colorado, 2009.

[12]Kastengren, A. L., Powell, C. F., Liu, Z., Moon, S., Gao, J., Zhang, X., and Wang, J., "Spray Diagnostics at the Advanced Photon Source 78-M Beamline," *22nd Annual Conference on Liquid Atomization and Spray Systems*, Cincinnati, Ohio, 2010.

[13]Lin, K.C., Carter, C., Smith, S., and Kastengren, A., "Exploration of Aerated-Liquid Jets Using X-ray Radiography," *50th AIAA Aerospace Sciences Meeting*, Nashville, Tennessee, AIAA 2012-0347, 2012.

[14]Halls, B. R., Heindel, T.J., Meyer, T.R., and Kastengren, A.L., "X-ray Spray Diagnostics: Comparing Sources and Techniques," *50th AIAA Aerospace Sciences Meeting*, Nashville, Tennessee, AIAA 2012-1055, 2012.

[15]Schumaker, S.A., Kastengren, A.L., Lightfoot, M.D.A., Danczyk, S.A., and Powell, C.F., "A Study of Gas-Centered Swirl Coaxial Injector Using X-ray Radiography," 12th *International Conference on Liquid Atomization and Spray Systems*, Heidelberg, Germany, 2012.

[16]Heindel, T. J., "A Review of X-ray Flow Visualization with Applications to Multiphase Flows," *Journal of Fluids Engineering*, Vol. 133, No. 7, 074001, 2011.

[17]Kastengren, A.L., Powell, C. F., Arms, D., Dufresne, E. M., Gibson, H. and Wang, J., "The 7BM Beamline at the APS: A Facility for Time-Resolved Fluid Dynamics Measurements," *Journal of Synchrotron Radiation*, Vol. 19, No 4, 2012, pp. 654-657.

[18]Berger, M.J., Hubbell, J.H., Seltzer, S.M., Chang, J., Coursey J.S., Sukumar, R., Zucker, D.S., and Olsen, K., XCOM: Photon Cross Sections Database, NIST Standard Reference Database 8 (XGAM), http://www.nist.gov/pml/data/xcom/index.cfm.

[19]Lightfoot, M.D.A., Schumaker, S.A., Villasmil, L.A., and Danczyk, S.A., "The Use of X-ray Radiography for Measuring Mass Distributions of Rocket Injectors," *JANNAF 8th Modeling and Simulation, 6th Liquid Propulsion, and 5th Space-craft Propulsion Joint Subcommittee Meeting*, Huntsville, Alabama, 2011, http://handle.dtic.mil/100.2/ADA554873 .

[20]Teshome, S., Leyva, I.A., Rodriquez, J., and Talley, D., "Geometry Effects on Steady And Acoustically Forced Shear-Coaxial Jet Sprays," *12th International Conference on Liquid Atomization and Spray Systems*, Heidelberg, Germany, 2012.

[21]Teshome, S., Leyva, I.A., Talley, D., and Karagozian, A.R. "Cryogenic High-Pressure Shear-Coaxial Jets Exposed to Transverse Acoustic Forcing," *50th AIAA Aerospace Sciences Meeting*, Nashville, Tennessee, AIAA 2012-1265, 2012.

[22] Kastengren, A., Powell, C.F., Wang, Y.-J, IM, K.-S., and Wang, J., "X-ray Radiography Measurements of diesel Spray Structure at Engine-Like Ambient Density," *Atomization and Sprays*, Vol. 19, No. 11, 2009, pp. 1031-1044.

[23]Teshome, S., "Droplet Combustion and Non-Reactive Shear-Coaxial Jets with Transverse Acoustic Excitation Thesis," Ph.D. Dissertation, Mechanical Engineering Dept., University of California, Los Angeles, CA, 2012.

[24]Woodward, R.D., Burch, R.L., Huo, K.K., and Cheung, F.-B. ,"Real-Time X-ray Radiography Study of Liquid Jet Breakup From Rocket Engine Coaxial Injectors." *International Journal of Energetic Materials and Chemical Propulsion*, Vol. 3, 1994, pp. 365-378.

[25] Eroglu, H., Chigier, N., & Farago, Z., "Coaxial atomizer liquid intact lengths," *Physics of Fluids A: Fluid Dynamics*, Vol. 3, No. 2, 1991, pp. 303-308.

[26]Leyva , I.A., Chehroudi, B., and Talley, D., "Dark core analysis of coaxial injectors at sub-, near-, and supercritical pressures in a transverse acoustic field," 43rd AIAA/ASME/SAE/ASEE Joint Propulsion Conference, AIAA 2007-5456, 2007.
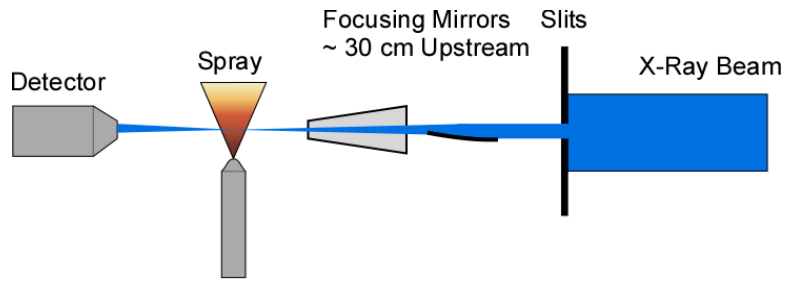
Figure 1. Sketch of the X-ray radiography experimental setup. Note that a titanium foil detector (not pictured) which measures beam intensity based on fluorescence emitted from the titanium foil was located in the beam path between the spray and the focusing mirrors.
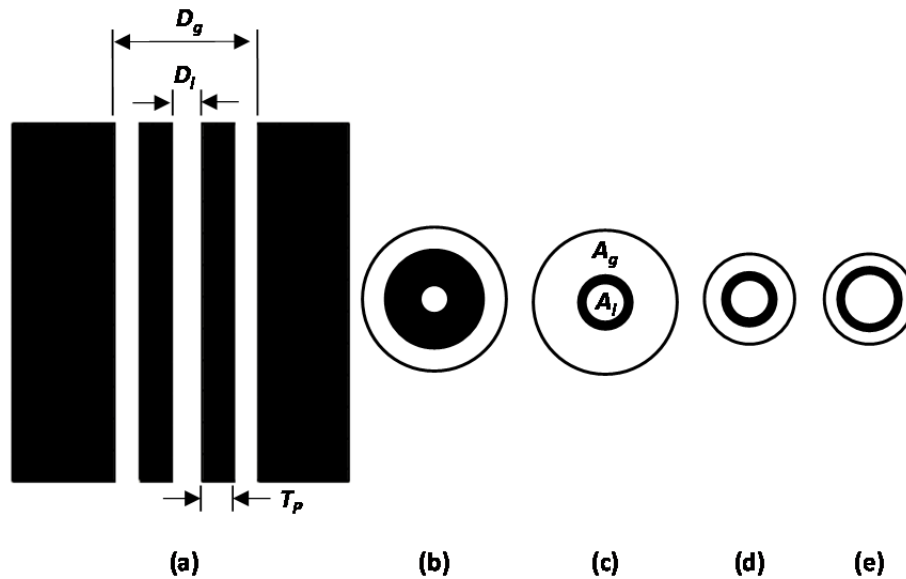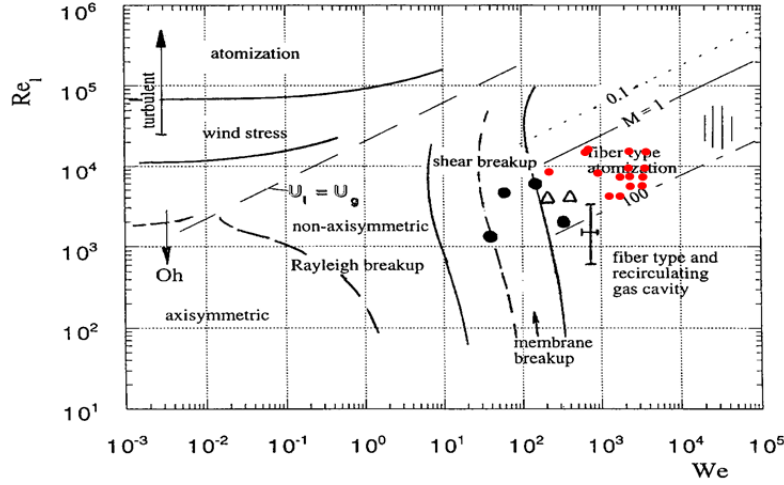

Figure 2. Injector schematic: (a) cross-sectional view, (b) Injector SC1, (c) Injector SC4, (d) Injector SC24 & (e) Injector SC2.



Figure 3. Photo of injector assembly.

Table 1. Injector dimensions.

Injector	D_l (mm)	D_g (mm)	T_p (mm)	L_l/D_l	T_p/D_l	A_g/A_l
SC1	2.08	10.2	2.32	48.8	1.12	13.4
SC4	2.79	10.2	0.457	36.4	0.164	11.5
SC24	2.79	6.35	0.457	36.4	0.164	3.40
SC2	3.61	6.35	0.432	28.2	0.120	1.56

Figure 4. Shear Coaxial Atomization Regime Diagram from Lasheras & Hopfinger (2000).[7] Test conditions for current represented by red points.

Table 2. Test conditions with mass flow rates and relevant nondimensional parameters.

| Condition	J	U_g (m/s)	U_l (m/s)	$\dot{m}_g$ (g/s)	$\dot{m}_l$ (g/s)	m	We	Re_g	Re_l
SC1-0.5	0.46	81	4.0	4.16	13.6	3.27	211	8,920	8,370
SC1-2	1.9	162	4.0	8.53	13.6	1.59	872	18,800	8,260
SC1-5	4.8	220	3.5	12.0	11.8	0.98	1667	27,600	7,290
SC1-10	9.6	182	2.0	9.62	6.79	0.71	1100	21,400	4,210
SC1-15	14	219	2.0	12.0	6.79	0.57	1651	27,300	4,240
SC2-0.5	0.48	121	6.0	2.27	61.2	27.0	850	7,670	20,800
SC2-2	1.8	202	5.5	4.25	26.1	13.2	2665	14,900	19,000
SC2-5	4.51	203	3.5	4.27	35.3	8.27	2683	15,000	11,800
SC2-10	8.7	204	2.5	4.26	25.5	6.00	2699	14,800	8,740
SC2-15	13.7	202	2.0	4.23	20.2	4.8	2656	14,800	7,290
SC4-0.5	0.49	125	6.0	9.85	36.7	3.72	673	25,800	15,700
SC4-2	2.0	229	5.5	18.4	33.6	1.82	2310	50,600	14,500
SC4-5	4.8	224	3.5	18.5	21.4	1.16	2260	51,800	9,150
SC4-10	9.1	219	2.5	18.4	15.4	0.84	2200	52,000	7,050
SC4-15	15	224	2.0	18.4	12.0	0.65	2250	51,400	5,590
SC24-0.5	0.46	120	6.0	2.88	36.7	12.7	635	10,400	16,500
SC24-2	1.8	212	5.6	5.40	34.3	6.34	2104	20,100	16,000
SC24-5	4.6	210	3.5	5.51	21.4	3.88	2120	21,000	9,340
SC24-10	8.7	211	2.5	5.44	15.4	2.83	2110	20,400	7,310
SC24-15	15	213	2.0	5.48	11.9	2.18	2140	20,700	5,550

American Institute of Aeronautics and Astronautics
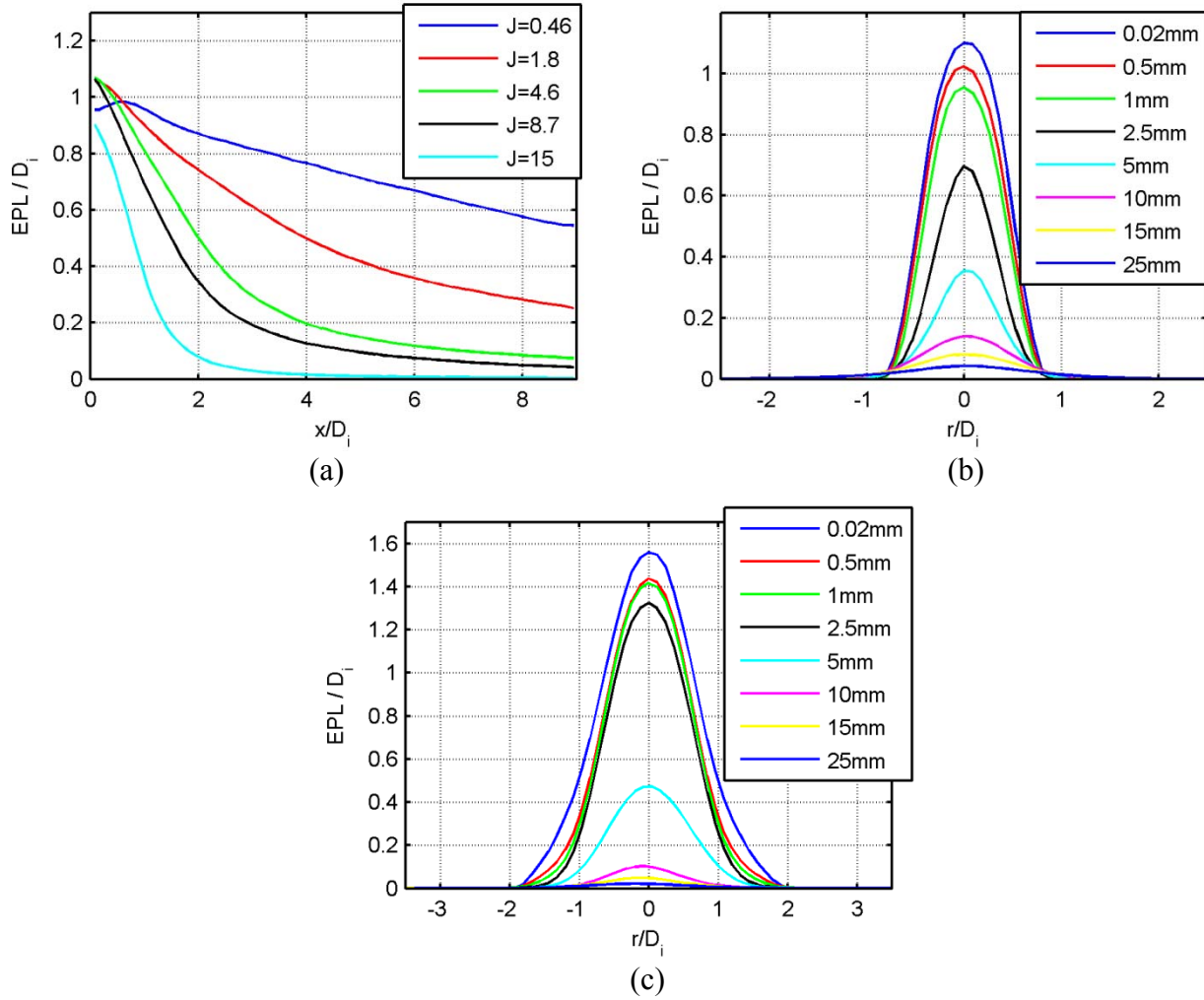
Figure 5. (a) Normalized centerline EPL profiles for injector SC24. (b) Normalized radial EPL for test condition SC24-10. (c) Normalized radial EPL for test condition SC1-10.
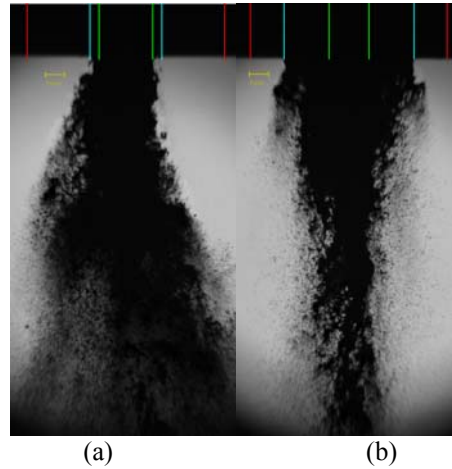

Figure 6. Instantaneous backlit images of test condition (a) SC4-10 and (b) SC1-10. Green lines mark the walls of the inner jet, blue lines mark the outer walls of the inner injector post, and red line mark the outer walls of the outer jet.
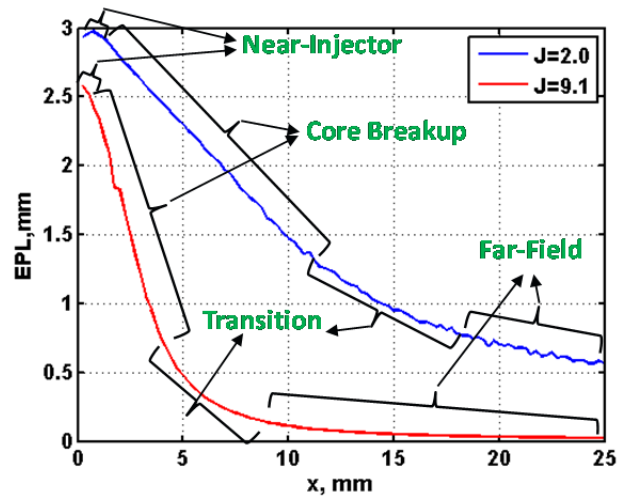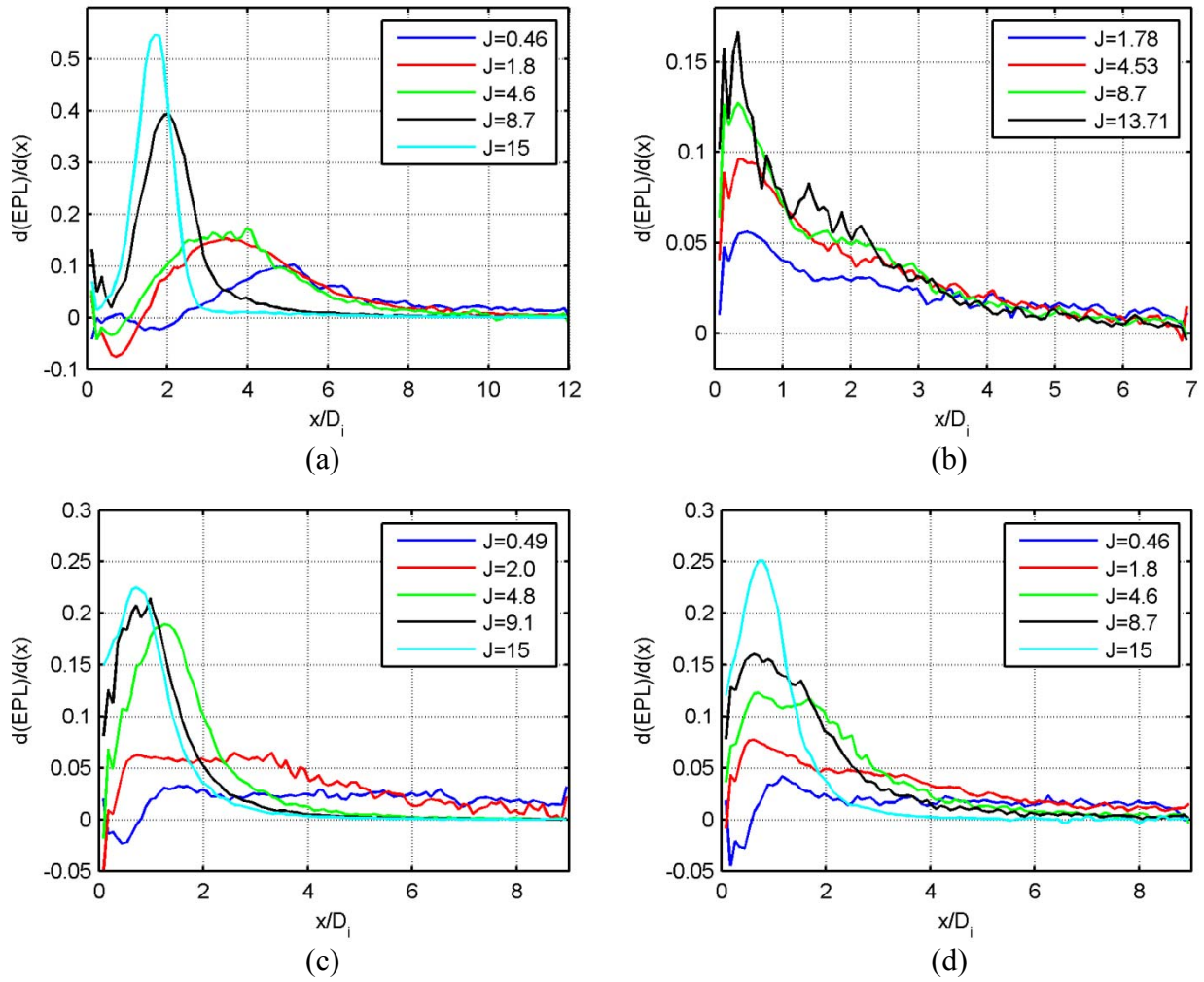
Figure 7. Centerline EPL profiles for test conditions SC4-2 and SC4-10 with hypothetical atomization regions labeled.
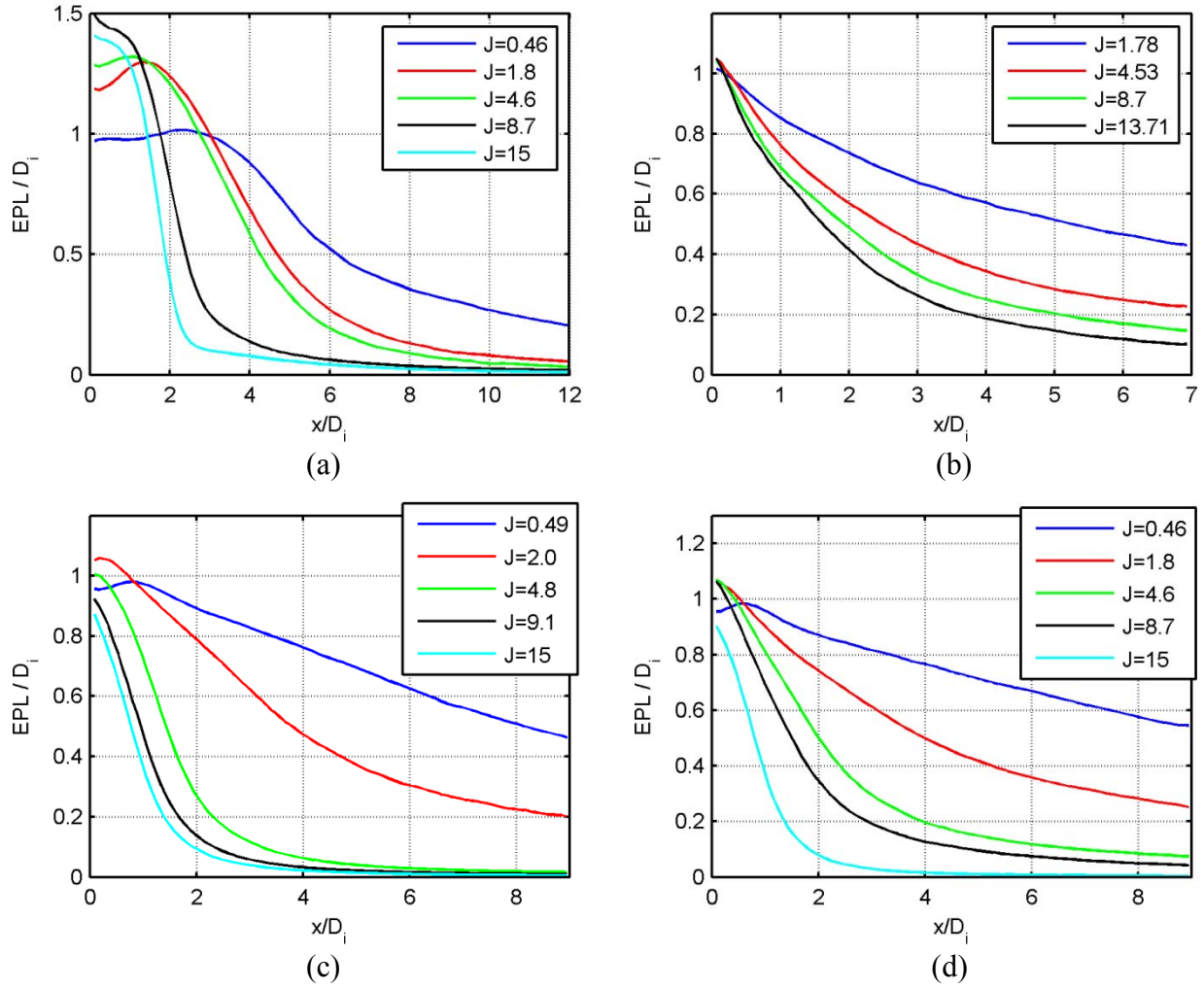
Figure 8. Normalized centerline EPL profiles for injector geometries (a) SC1, (b) SC2, (c) SC4 and (d) SC24.
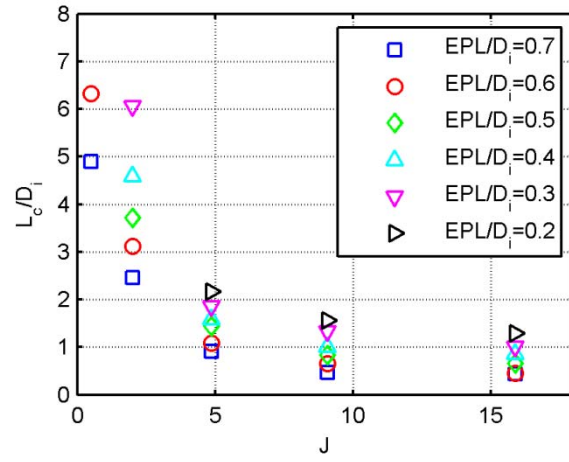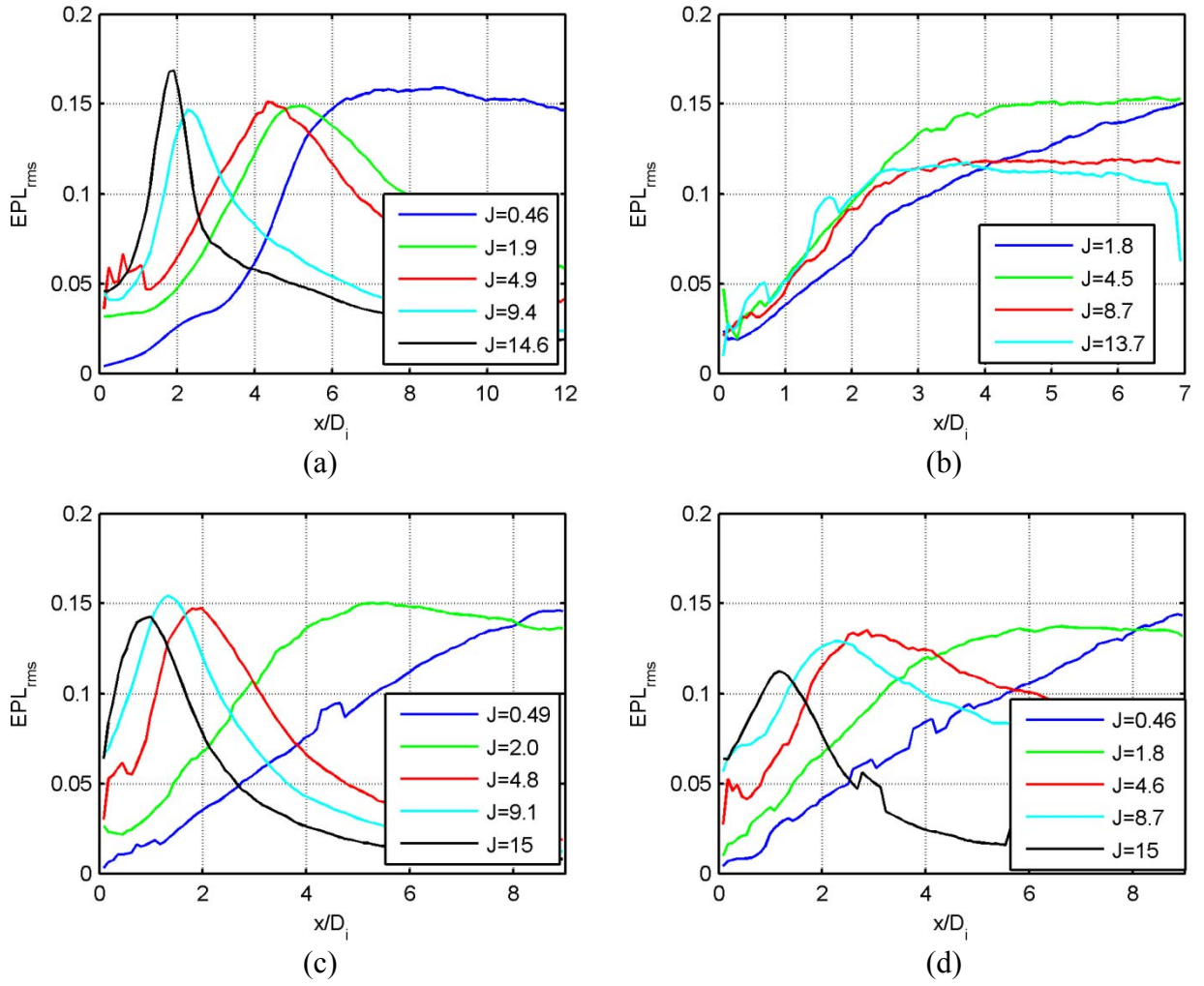
Figure 9. Normalized core lengths versus *J* for different normalized EPL levels for injector geometry SC4
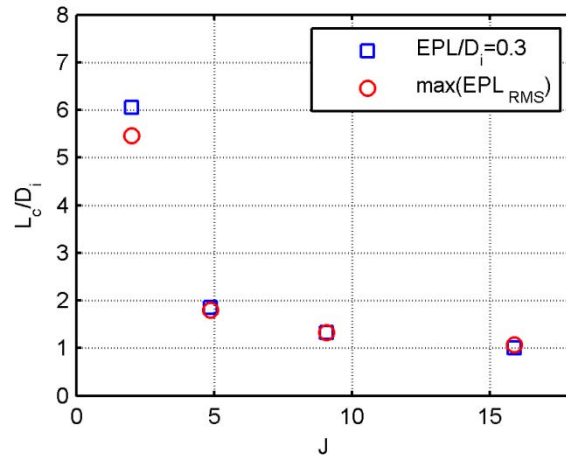

(a)

(b)

(c)

(d)

Figure 10. Spatial derivative of the centerline EPL profiles for injector geometries (a) SC1, (b) SC2, (c) SC4 and (d) SC24.
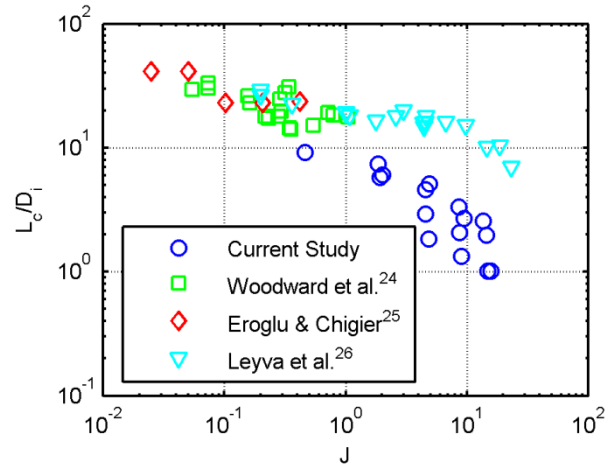
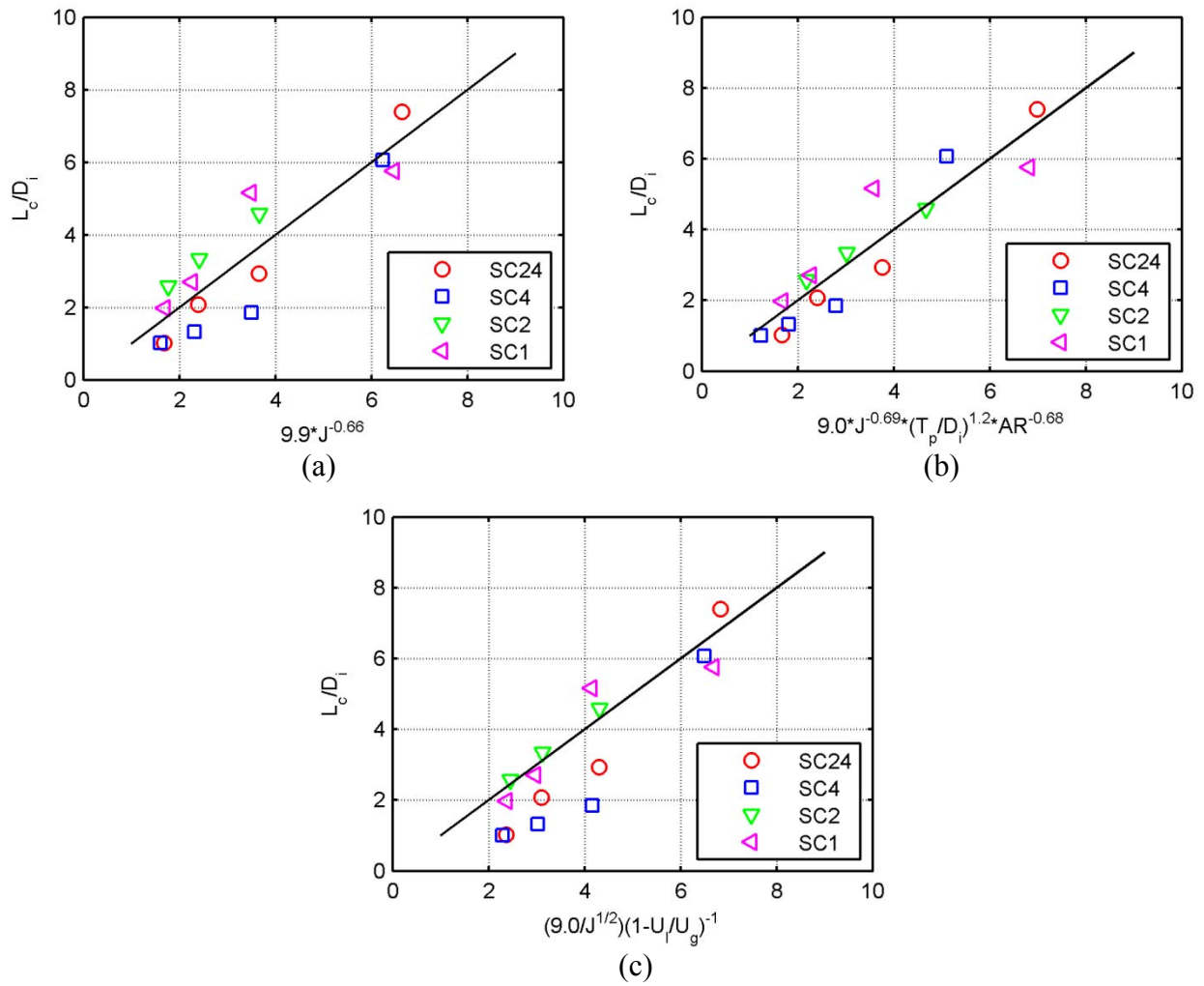**Figure 11.** Centerline EPL RMS profiles for injector geometries (a) SC1, (b) SC2, (c) SC4 and (d) SC24.

Figure 12. Two methods to measure the core length, *EPL/D_i=0.3* and the maximum centerline EPL$_{RMS}$ are compared for injector SC4.

Figure 13. Normalized core lengths for the current study compared with two-phase core length data from the literature.

(a)

(b)

(c)

Figure 14. Linear regression fits for normalized core length data. (a) Standard momentum flux ratio fit, (b) momentum flux ratio with area ratio and post thickness ratio suggested by Teshome,[23] and (c) momentum flux ratio with velocity ratio suggested by Lasheras and Hopfinger.[7]